tion type, fair agreement is obtained. Detailed agreement, for all energies for which the measurements have been made, however, is not very good for all nuclides. There is some evidence of a fluctuation in the S-wave strength function for the nuclides investigated rather than the smooth values as a function of A expected from the optical model.

It also seems likely that the S- and P-wave parameters for the optical model may be different, and this could possibly account for the present lack of detailed agreement of the model with our data. More accurate measurements of the S-wave total neutron cross section in the low-energy range ($\lesssim 10$ keV) would be desirable as a check of this conclusion. The many-body calculation of Gomes for nuclear matter suggests that surface absorption should play a large part in forming the compound nucleus at low-incident neutron energies. The better agreement of the present data with the surface absorption (rather than volume absorption) model supports this prediction. Because of the requirement of a large imaginary potential in interpreting our data, it is not possible to differentiate between spin-orbit strengths of 8 or 16 MeV. However, no potential within this range would show a splitting of the P-wave strength function near $A \cong 100$.

ACKNOWLEDGMENTS

The measurements reported in this paper were carried out at the NRU reactor in Chalk River, Canada, using the joint BNL-AECL fast chopper facility. We wish to thank our many colleagues at Chalk River for the help they provided in setting up this joint facility which made these measurements possible.

PHYSICAL REVIEW VOLUME 137, NUMBER 1B 11 JANUARY 1965

Prompt Neutrons from Thorium Photofission*

C. P. SARGENT, W. BERTOZZI, P. T. DEMOS, J. L. MATTHEWS, AND W. TURCHINETZ
Department of Physics and Laboratory for Nuclear Science, Massachusetts Institute of Technology, Cambridge, Massachusetts

(Received 27 March 1964; revised manuscript received 10 September 1964)

We have measured the distribution in angle and velocity of the prompt neutrons from the bremsstrahlung-induced photofission of Th^{232} in the photon energy region near threshold. Using knowledge of the fission-fragment angular distribution, the data have been interpreted in terms of the neutron distribution relative to the fragment axis. The measurement allows a quantitative estimate of the fraction of neutrons which are not emitted by fully accelerated fragments. The result for this fraction is 0.07 ± 0.09. Assuming isotropic neutron emission in the fragment center-of-mass frame, the analysis also determines some characteristics of the neutron energy spectrum in this frame. The spectrum has an average energy $\bar{\eta} = 1.14 \pm 0.06$ MeV and a second central moment $\sigma^2(\eta) = (0.77 \pm 0.06)\bar{\eta}^2$. If it is represented by an evaporation-type spectrum with some distribution of temperatures, there is no significant contribution from temperatures equal to or greater than $\bar{\eta}$. We have made a similar analysis of data on prompt neutrons from the spontaneous fission of Cf^{252} obtained by Bowman, Thompson, Milton, and Swiatecki, and compared the results with those for Th^{232} photofission.

I. INTRODUCTION

THE recent rapid progress in the development of experimental techniques has provided a qualitative change in the experimental understanding of prompt-neutron emission in the fission process.[1–3] The most comprehensive prompt-neutron measurements reported to date are those of Bowman, Thompson, Milton, and Swiatecki,[1] in which neutrons from the spontaneous fission of Cf^{252} were measured in coincidence with the fission fragments by a triple time-of-flight technique. Their results may be summarized as follows: (a) Most of the neutrons observed are emitted from fully accelerated fragments with an angular distribution which is isotropic in the center-of-mass frame of the moving fragment (henceforth abbreviated "c.m. frame"). (b) The shape of the energy distribution in the c.m. frame is independent of fragment mass A and kinetic energy E_k of the fission event, over a wide range of A and E_k. (c) Therefore, the prompt neutrons as observed (fragment charge, for example, is not observed) may be characterized by two functions of A and E_k, $\nu(A,E_k)$ and $\bar{\eta}(A,E_k)$, where ν is the number of neutrons emitted and $\bar{\eta}$ the average c.m. neutron energy. These functions have been determined for the Cf^{252} spontaneous-fission neutrons.[1] The strong A dependence of ν has been known

* This work is supported in part through funds provided by the U. S. Atomic Energy Commission under Contract AT(30-1)-2098.

[1] H. R. Bowman, S. G. Thompson, J. C. D. Milton, and W. J. Swiatecki, Phys. Rev. **126**, 2120 (1962); **129**, 2133 (1963). These references will be referred to as BTMS.

[2] S. S. Kapoor, R. Ramanna, and P. N. Rama Rao, Phys. Rev. **131**, 283 (1963).

[3] K. Skarsvåg and K. Bergheim, Nucl. Phys. **45**, 72 (1963).

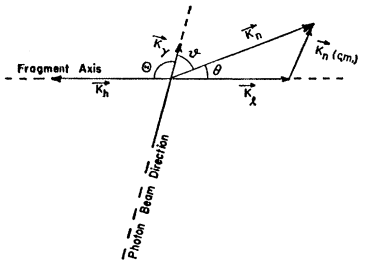

FIG. 1. Definition of angles in the photofission-neutron experiment.

for some time[4]; experimental results on this subject have been summarized by Terrell.[5]

An important result of the new knowledge of the overall nature of the neutron and fragment distributions is to increase the attractiveness of less comprehensive experiments which are especially sensitive to some particular feature of the fission process. These now, with more confidence, can be interpreted in terms of that feature against the background of sensitivities to many other features. Such an experiment is the one reported here on the distribution in energy and in angle relative to the incident photon beam of the prompt neutrons emitted in the photofission of Th^{232} near threshold. A primary motivation for the experiment is simply that no measurements of photofission prompt-neutron spectra have been reported.

The results of any photofission neutron experiment which detects only the neutron are unambiguous only in the threshold region, since the only discrimination against neutrons from the (γ,n) reaction is the requirement that $E_n(\gamma,f)>E_\gamma-S_n$, where $S_n=6.0$ MeV for Th^{232}.[6] The most striking characteristic of photofission of even-mass nuclei near threshold is the strong angular dependence of the fragment direction relative to the photon beam.[7,8] The fragment angular distribution is of dipole form $(a+b\sin^2\Theta)$ (see Fig. 1) and, for Th^{232}, b/a remains much larger than one for fissions induced by bremsstrahlung with maximum energy as high as 9 MeV.[8] The existence of this fragment anisotropy allows us to interpret a neutron angular distribution, measured relative to the incident photon direction, in terms of the distribution of neutrons relative to the fragment direction.

It is useful to discuss the experiment in terms of the function $\rho(v,\theta)$ used in BTMS, the density of neutrons in laboratory velocity space normalized to the total number of neutrons emitted per fission. θ is the angle between the neutron velocity v and the direction of, say, the light fragment. For Cf^{252}, ρ was measured as a function of v, θ, fragment-mass ratio, and total kinetic energy released in the fission process. The ρ discussed in this paper is integrated over mass ratio and energy release.

Only certain angular moments of ρ are measured for Th^{232} photofission in the present experiment. Let ρ be expanded as a series in the Legendre polynomials

$$\rho(v,\theta)=\rho_0(v)[1+\sum_{n=1}^{\infty}\rho_n(v)P_n(\hat{k}_n\cdot\hat{k}_l)], \qquad (1)$$

where $\hat{k}_n$ is a unit vector in the neutron direction, $\hat{k}_l$ is a unit vector in the light fragment direction in the laboratory, and $\hat{k}_n\cdot\hat{k}_l=\cos\theta$. The fragment angular distribution relative to $\hat{k}_\gamma$, the incident photon direction, is proportional to $1+a_2P_2(\hat{k}_l\cdot\hat{k}_\gamma)$, with $a_2=-(b/a)\times[(\frac{3}{2})+(b/a)]^{-1}\approx-1$ near the photofission threshold.[7,8] The neutron density in laboratory velocity space for photofission is then proportional to $n(v,\vartheta)$, where

$$n(v,\vartheta)v^2dv=\rho_0(v)v^2dv[1+\tfrac{1}{5}a_2\rho_2(v)P_2(\cos\vartheta)]. \qquad (2)$$

$4\pi\rho_0(v)v^2dv$ is the total (integrated-over-angle) distribution in neutron speed and $\cos\vartheta=(\hat{k}_n\cdot\hat{k}_\gamma)$.

With the knowledge of a_2,[7,8] a measurement of the neutron velocity spectrum at two angles (preferably one near 90° and the other near 0 or 180°) determines $\rho_2(v)$, the second angular moment of ρ, in a manner which depends only on the ratio of the number of neutrons counted at one angle to the number counted at the other angle. The observed ρ_2 depends then only on the ratio of the detector efficiencies at a given neutron velocity. If the velocity dependence of the efficiency is known, the measurement also determines ρ_0 to within a constant factor.

Measurements at $\vartheta=157°$ and $\vartheta=77°$ have been made of the Th^{232} neutron spectrum using bremsstrahlung of maximum energy 6.75 MeV and 7.75 MeV from the MIT linear accelerator. The spectra were investigated at the two angles simultaneously by the time-of-flight technique over 9.3-m flight paths, and the counter efficiencies determined by a method which will be described. Some spectra have also been measured at 130 and 50°. In analyzing the resulting data, the point of view is adopted that, until there is reason to believe otherwise, photofission at threshold should be considered similar to any threshold fission process—slow-neutron-induced fission or spontaneous fission, for example—as far as the prompt neutrons are concerned. In this spirit the results are compared rather directly with those of BTMS, in the hope of illuminating further the neutron emission process, in particular the hypothesis of emission from fully accelerated fragments. This question is often phrased, "How many neutrons are 'scission neutrons'?" The majority of the prompt neutrons ("fission neutrons") are presumably emitted between times of the order of 10^{-20} and 10^{-14} sec after fission, whereas scission neutrons are said to be emitted in times $\lesssim 10^{-21}$ sec. The fast emission could occur as a result of the rather violent

[4] J. S. Fraser and J. C. D. Milton, Phys. Rev. **93**, 818 (1954).
[5] J. Terrell, Phys. Rev. **127**, 880 (1962), with errata, **128**, 2925 (1962).
[6] D. M. Van Patter and W. Whaling, Rev. Mod. Phys. **26**, 402 (1954).
[7] E. J. Winhold, P. T. Demos, and I. Halpern, Phys. Rev. **87**, 1139 (1952); A. W. Fairhall, I. Halpern, and E. J. Winhold, *ibid.* **94**, 733 (1954).
[8] A. P. Baerg, R. M. Bartholomew, F. Brown, L. Katz, and S. B. Kowalski, Can. J. Phys. **37**, 1418 (1959).

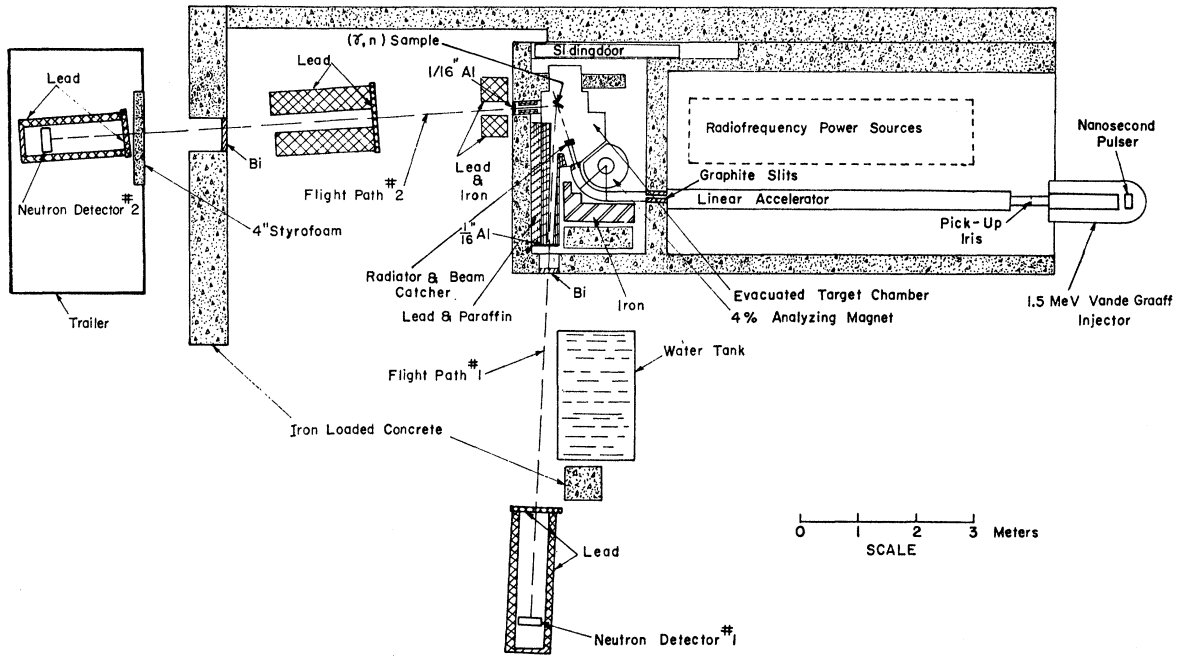

FIG. 2. Photoneutron time-of-flight setup at the MIT Linear Accelerator. Neutrons are detected at two angles simultaneously. For most of the experiment, the angles were 77 and 157° relative to the bremsstrahlung beam.

changes in nuclear shape accompanying the snapping of the neck at scission.[9] These neutrons are presumed to have a distribution relative to the fragment axis which is more nearly isotropic than that of the fission neutrons, the latter being a strongly forward-and-back peaked distribution arising from the addition of the relatively large fragment velocity to the c.m. neutron velocity. Another source of neutrons isotropic in the laboratory has been proposed recently by Kapoor, Ramanna, and Rama Rao.[2] They suggest that neutrons may be evaporated during the time it takes the fissioning nucleus to go from the saddle point to scission, and that this may be a significant source of neutrons if this time is as long as 10^{-20} sec. These pre-scission neutrons should be experimentally indistinguishable from the scission neutrons defined above, and will hereafter be included under the latter term.

With an experiment which measures $\rho(v,\theta)$, the scission neutron problem may be approached in the following way. First the c.m. velocity distribution of the fission neutrons (which certainly represent most of the neutrons) must be known, and is perhaps best determined by observing $\rho(v,180°)$ and $\rho(v,0°)$. At these angles the domination of the fission neutrons over the scission neutrons should be most complete, and the c.m. speed is obtained simply by subtracting the appropriate fragment speed from the observed neutron speed. The contribution to ρ of the other fragment emitting neutrons backward relative to its velocity is a small correction for speeds greater than about 1 cm/nsec. The angular distribution of fission neutrons in the c.m. frame can be determined by close examination of the rapid fall in ρ with angle as θ is increased from 0° or decreased from 180°. Finally, with this information the number of neutrons which should be observed near 90° if there are no scission neutrons may be predicted and compared with experiment.

In terms of the angular moments of $\rho(v,\theta)$ defined above, over the velocity range from about 1–3 cm/nsec, ρ_0, the total neutron spectrum, is relatively insensitive to everything except the average energy of emission. ρ_4 and the higher even moments are especially sensitive to the angular distribution of fission neutrons in the c.m. frame. At very high velocities, all the even moments are very dependent upon the emission spectrum at high c.m. energies. The odd moments are measures of the various possible asymmetries between neutrons emitted by heavy and by light fragments. This leaves ρ_2 as probably the most useful moment for observing scission neutrons. These remarks can be understood by examination of Fig. 1, and will be illustrated quantitatively when the experimental results are discussed.

The measured values of ρ_0 and ρ_2 for Th^{232} photofission are compared with the results expected under the assumption of neutron evaporation from fully accelerated fragments. The measurements imply that probably a few percent of the neutrons are scission neutrons within the range of velocities considered. The sensitivity of this conclusion to the parameters entering in the evaporation prediction has been investigated. A

[9] D. C. Hill and J. A. Wheeler, Phys. Rev. **89**, 1102 (1958); R. W. Fuller, *ibid.* **126**, 684 (1962).

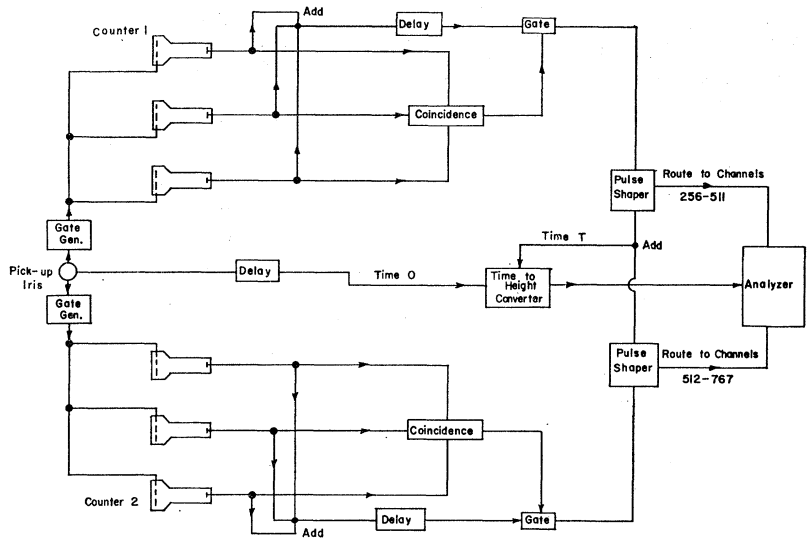

FIG. 3. Block diagram of time-of-flight electronics.

significant amount of information concerning the c.m. emission spectrum can be obtained from the analysis. The data of BTMS have been integrated over angle and the angular moments of ρ determined for Cf^{252} in order to allow a direct comparison of the Th^{232} and Cf^{252} measurements.

2. EXPERIMENTAL APPARATUS

The experimental layout is shown schematically in Fig. 2. As a source of γ rays the pulsed bremsstrahlung beam from the MIT linear electron accelerator[10] was used. The electron gun at the high-voltage end of the 1.5-MeV Van de Graaff injector is driven into conduction by a pulser which produces bursts of electrons several nanoseconds wide at a repetition rate of 120 pulses per second. About 0.75-A peak current is injected into the first radio-frequency section of the linac, of which 150 mA is accelerated to full machine energy, with a spread of about 10%. The electrons are energy-analyzed to 4% by a deflecting magnet, yielding peak currents of about 40 mA. Bremsstrahlung is produced by a 0.4-g/cm^2 tantalum-foil radiator backed by a 5-cm block of carbon. The beam is monitored by integrating the current caught on the carbon block.

The fission sample, located about 12 in. from the bremsstrahlung source, consisted of a stack of one hundred $1\frac{1}{2}$in.$\times 1\frac{1}{4}$ in.$\times 0.004$ in. foils, bound with black tape and mounted on aluminum rods. The useful target thickness is limited by γ-ray absorption, and its area by the size of the beam and collimators. The target chamber is evacuated in order to reduce background due to the annihilation radiation from positrons which are produced copiously in the bremsstrahlung target and carbon backing.[11]

Paraffin collimators serve to define the source of the neutrons, and iron, lead, and concrete shielding prevents scattered γ rays originating in the target area from reaching the detectors. Lead and bismuth absorbers are placed in the neutron flight paths to reduce further the γ-induced background.

Two identical neutron detectors are placed at 77 and 157° with respect to the γ-ray beam. The 77° counter is located outside the accelerator building in a trailer, for which a 4-in. sheet of styrofoam provides a light-weight door. The detectors are brass cylinders 14 in. in diameter and 5 in. deep (inside dimensions), which are coated with MgO and filled with a scintillating solution consisting of toluene activated by 4.4 g/liter p-terphenyl. As a wavelength shifter, 0.15-g/liter POPOP is added. Neutrons enter along the axis of symmetry. On the opposite face are mounted three RCA 7046 14-stage photomultipliers. The phototubes are normally biased off, being gated on for 1 μsec beginning 135 nsec after the γ-ray flash occurring with each beam pulse.

A simplified block diagram of the electronics is shown in Fig. 3. Neutron energies are measured by the time-of-flight technique, the flight time being electronically converted to a pulse height. Before entering the first rf section of the linac, the electron burst passes through an iris, producing a voltage pulse. This pulse triggers the phototube gate generator and also starts a constant-current generator (at "time 0"), generating a voltage signal rising linearly with time. The output of the three-phototube coincidence circuit serves to turn off the constant-current generator (at "time t"), and the volt-

[10] P. T. Demos, A. F. Kip, and J. C. Slater, J. Appl. Phys. **23**, 53 (1952).

[11] W. Bertozzi, P. T. Demos, S. Kowalski, F. Paolini, C. P. Sargent, and W. Turchinetz, Nucl. Instr. Methods (to be published).

age signal is then fed into a 1024-channel pulse-height analyzer. By suitable coding of the signals from each detector, those from the 157° counter are analyzed in one group of 256 channels and those from the 77° counter in another group of 256 channels. The time-to-height converter responds to the first event in either counter associated with a given accelerator beam burst. The counting rates are sufficiently low that it is unlikely for two detector events to be associated with the same beam burst. To measure such dead-time effects a third group of 256 channels records the spectrum of events in which a count in each of the two detectors occurred during the 1 μsec gating interval. The use of two counters, to measure the spectra at two angles simultaneously, eliminates errors in the angular distribution parameter arising from inaccurate beam monitoring. The use of one time-to-height converter and one analyzer (with one analog-to-digital converter) avoids intrasystem calibration problems. For a more detailed discussion of the experimental techniques and electronics, we refer to a forthcoming paper.[11]

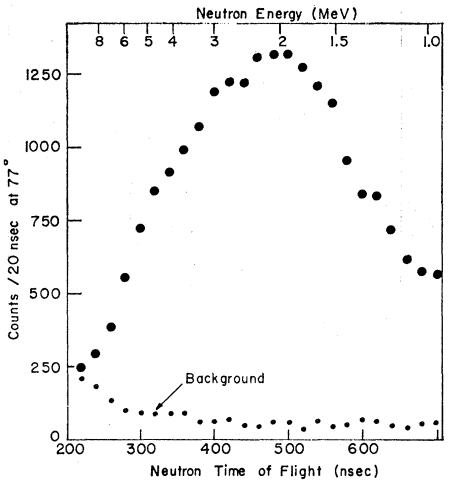

FIG. 4. Thorium photoneutron time-of-flight spectrum observed at 77° with 7.75-MeV bremsstrahlung. The points labeled "background" are the normalized result of a run with a bismuth target.

3. EXPERIMENTAL PROCEDURE

The time-of-flight apparatus is calibrated by triggering the phototube gate generator with a pulse synchronized with the accelerator beam burst, so that the tubes are operative when γ rays produced and scattered in the neighborhood of the fission sample reach the detector. This produces a line in the time spectrum which can then be translated across the analyzer scale by inserting calibrated cables, whose electrical lengths are known to about 1%, in series with one or the other input of the time-to-height converter. Over-all linearity of the system is checked by measuring the flat time spectrum produced by a radioactive source placed near a detector. Since flight-path lengths and γ-ray flight times are known, the above procedure determines the neutron velocity calibration. This method of calibration has been checked by the positions of features of the C^{12} total neutron cross section measured when a neutron spectrum is observed in transmission through carbon. We believe that the absolute velocity scale is accurate to 1% for velocities greater than 2 cm/nsec, the precision decreasing to about 2% at 1 cm/nsec. The relative calibration of one detector versus the other is considerably more precise.

The thorium target was attached to one arm and an approximately equal mass of bismuth attached to the other arm of a double target holder which enabled either sample to be rotated into position without opening the target chamber. The bismuth was placed in the beam to provide a high-Z γ-ray scatterer in order to obtain a reliable background estimate. The bremsstrahlung energies were too low to produce $\mathrm{Bi}(\gamma,n)$ neutrons in the velocity range of interest. In fact, in that range the background was nearly independent of whether bismuth or no sample was in the target position.

Figure 4 illustrates the flight-time distributions observed at 77° with 7.75-MeV bremsstrahlung. The background points are the results of a bismuth run normalized to the integrated beam intensity of the thorium run on the basis of charge collected on the carbon beam stopper. The flat-in-time component of the background which predominates at the longer flight times is running-time correlated rather than beam correlated. Corrections to the charge-normalized background were made where necessary on the basis of a measurement of the background rate with the accelerator off, and the charge to running-time ratios for the thorium and bismuth runs. The remaining background is proportional to integrated current over the time range of interest. This background seems to be due to γ rays produced by electrons accelerated considerably later than the main beam burst.

The profile of the beam burst as observed during calibration is flat-topped with a full width of 20 nsec, and in good approximation represents the time resolution function during the experiment.[11] This experiment did not require particularly high resolution and in the interest of high counting rate the electron gun was operated with a conduction interval several times the minimum width available. The thorium data of Fig. 4 were accumulated in about 15 h of beam time.

Owing to the strong dependence of the fission-fragment angular distribution on E_0, the maximum energy of the bremsstrahlung spectrum,[8] the interpretation of the data requires reasonably precise definition of this endpoint energy The flip coil in the field of the beam analyzing magnet is normally calibrated by measurement of the neutron spectrum from the photodisintegration of deuterium. E_0 is then defined as that energy for which a theoretical bremsstrahlung spectrum shape of

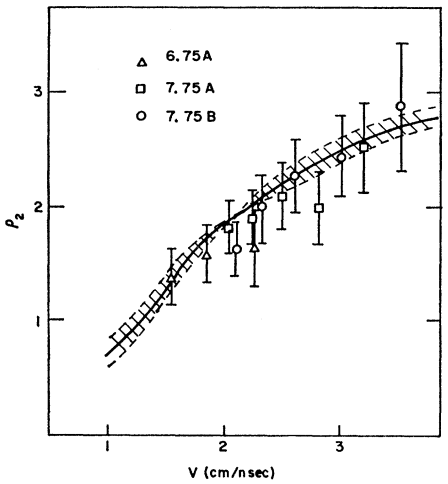

FIG. 5. Second angular moment ρ_2 of the neutron distribution relative to the fragment axis for Th^{232} photofission, plotted as a function of neutron velocity v. This quantity is determined by the ratio of the numbers of neutrons observed at $\vartheta=77°$ and $\vartheta=157°$, by the ratio of the efficiencies of the detectors, and by the fragment anisotropy parameter. The labels 6.75A, 7.75A, and 7.75B indicate the bremsstrahlung endpoint energy in MeV and the method used to determine the relative counter efficiencies (see text). The solid curve represents a prediction for ρ_2 on the basis of isotropic evaporation from moving fragments. The curve and the significance of the shaded region are discussed in the text.

the Schiff type[12] with maximum energy E_0 most nearly produces the observed $H^2(\gamma,n)H^1$ neutron spectrum corrected for the energy dependence of the cross section and of the counter efficiency and for the 4% spread in electron energy allowed by the magnet.

Some preliminary results of this experiment have been reported.[13] These early data are of less statistical significance than the present data and are not included in the results given here. Three experiments, labeled 7.75A, 6.75A, and 7.75B, will be discussed. The numerical part of the label is E_0, the maximum bremsstrahlung energy, and the A and B experiments differ in the method used to determine the relative efficiencies of the 157 and 77° counters. These methods will be described in the next section.

4. TREATMENT OF THE DATA

The ratio of the thorium spectra observed in the two counters at neutron velocities higher than the maximum possible velocity for the (γ,n) process determines ρ_2, the second angular moment of the prompt-neutron velocity distribution as defined above [Eqs. (1) and (2)]. Let $N(v,\vartheta)$ be the number of counts per unit flight-time interval observed at angle ϑ relative to the the photon beam. $N(v,\vartheta)$ is proportional to the quantity $g(v,\vartheta)n(v,\vartheta)v^4$, where $g(v,\vartheta)$ is the detection efficiency function. From Eq. (2)

$$\rho_2(v)=-\frac{5}{a_2}\left[\frac{R-1}{RP_2(\cos157°)-P_2(\cos77°)}\right]$$
$$=-\frac{5}{a_2}\left[\frac{R-1}{0.76R+0.43}\right], \quad (3)$$

with

$$R\equiv[N(v,77°)/N(v,157°)][g(v,157°)/g(v,77°)]$$
$$\equiv\epsilon N(v,77°)/N(v,157°).$$

ϵ may differ from unity because of geometrical asymmetries between the two flight paths or counters or because of electronic differences in the counters. a_2, the angular distribution parameter of the fragments relative to the incident γ-ray direction, is found to be -0.83 ± 0.03 for $E_0=7.75$ MeV and -0.89 ± 0.03 for $E_0=6.75$ MeV.[8]

At the time the A runs were made ϵ was determined by comparing the angular distribution of photoneutrons from Be^9 (10-MeV bremsstrahlung) measured then with a similar angular distribution measured a year earlier. In the earlier experiment the efficiency ratio had been determined by repeating the Be^9 measurement with the counters interchanged and computing a small correction for slight differences in flight-path geometry. The ϵ for the A runs thus derived was found to differ considerably from unity, and it was subsequently discovered that one of the counters was not full of liquid scintillator solution. This should not affect the reliability of the results, however, since the Be^9 comparison was made and the Th^{232} data were taken under the same experimental conditions.

Run 7.75B was made five months later, with ϵ determined by a different method. At that time the same equipment was being used in a series of precise measurements of the angular distribution of the photoneutrons from deuterium.[14] Included were some experiments with the beam-analyzing magnet altered so that the counters were located at 50 and 130° relative to the photon direction. To determine ϵ, it was assumed that the neutrons emitted from uranium and thorium when bombarded with 9-MeV bremsstrahlung are symmetric about 90°.

The results of the experiments performed are consistent with this assumption. The ratio of counts observed at 130° to those observed at 50° with a thorium target is the same within statistical accuracy (about 1%) as the ratio observed with a uranium target. In the neutron energy range of interest (>2 MeV), most of the neutrons produced by 9-MeV bremsstrahlung are fission neutrons. In the fission process, neutrons emitted preferentially forward or backward relative to the photon beam in the laboratory could result from higher multipoles inter-

[12] A. S. Penfold and J. E. Leiss, *Analysis of Photo Cross Sections* (Physics Research Laboratory, University of Illinois, Urbana, Illinois, 1958).

[13] J. L. Matthews, W. Bertozzi, P. T. Demos, C. P. Sargent, and W. Turchinetz, Bull Am. Phys. Soc. 7, 303 (1962).

[14] D. McConnell, Ph.D. thesis, Massachusetts Institute of Technology, 1963 (unpublished).

fering with the predominantly electric dipole photon absorption and producing preferential emission of, say, the heavy fragment in the forward or backward hemisphere. Experiments on the fragment angular distribution have not been sensitive to such asymmetries. It is likely however that if small fore-aft asymmetries existed they would differ for thorium and uranium near threshold, since in this energy region the fissioning thorium nucleus passes through levels with sharper energy definition, producing much larger fragment anisotropies, compared with the uranium nucleus.[8]

Fore-aft symmetry is also implied by an experiment which compares the angular distributions of thorium neutrons, produced by 9-MeV bremsstrahlung, upon interchanging the lead and bismuth γ-ray filters in the two flight paths. If one assumes that the two counters are physically and electronically identical, and attributes small departures from unity for the 130° to 50° count ratio to a difference in the γ-ray filters, the result is that the neutrons are symmetric about 90°.

For run 7.75B, ϵ, derived from the fore-aft measurements, was equal to 1.03 ± 0.02 and constant over the energy range of interest.

The results for ρ_2 as a function of neutron velocity are shown in Fig. 5. Neutron energy in MeV is related to velocity in cm/nsec to a good approximation by $E=0.523v^2$. No corrections to the data have been made. Corrections for angular and energy resolution are very small. The correction for γ-ray absorption and neutron scattering in the target has been calculated by a digital computer code and is less than 3% in ρ_2 over the range. The errors shown for the points are in large part statistical. If one wishes to average several points, the systematic errors are about 6% in ρ_2, with approximately equal contributions arising from the uncertainty in a_2 and the uncertainty in ϵ. The curves displayed along with the data in Fig. 5 will be described in the next section.

Evaluating

$$N(v,\vartheta)\propto\rho_0(v)v^4g(v,\vartheta)[1+\tfrac{1}{5}a_2\rho_2(v)P_2(\cos\vartheta)],$$

at the two angles and eliminating the quantity $\frac{1}{5}a_2\rho_2(v)$, we find

$$\rho_0(v)v^4\propto[g(v,77°)]^{-1}\times[0.64N(v,77°)+0.36\epsilon^{-1}N(v,157°)]. \quad (4)$$

The energy dependence of the efficiency of the 77° counter for neutron energies less than about 6 MeV was determined by measuring with that counter the neutron spectrum produced from deuterium by 17.5-MeV bremsstrahlung. In the photodisintegration of the deuteron, there is a one-to-one correspondence at a given angle between the observed neutron flight time and the energy of the incident photon which produced the neutron, so that a neutron flight-time spectrum may be converted to a spectrum in incident γ-ray energy by the reaction kinematics. This spectrum, when divided by the product

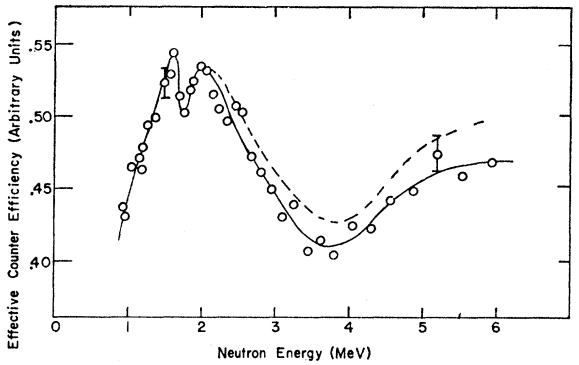

FIG. 6. Neutron detection efficiency function $g(E,77°)$ for the 77° counter. Note the suppressed zero. The solid curve is drawn by eye through the points; the dashed curve results from correcting the solid curve for thick target effects and is the efficiency function used in the experiment.

of the deuteron photodisintegration cross section at the proper angle and a function representing the energy dependence of the incident bremsstrahlung spectrum, is proportional to the efficiency of detection. Current theoretical predictions[15,16] for the energy dependence of the deuteron photodisintegration cross section near 90° should be reliable in the photon energy range between 3 and 15 MeV. The dominant $\sin^2\Theta$ term in the cross section has little sensitivity to anything except the binding energy of the deuteron and the triplet effective range. The other small terms have been investigated in this laboratory[14]; the results indicate good agreement with the theory. For the present purpose, the deuterium cross section was assumed to be that calculated by Partovi[15] on the basis of the Hamada potential for the two-nucleon interaction, which agrees well with other recent calculations[16] and with experiment[17] in the energy range of interest. For 17.5-MeV bremsstrahlung (the highest energy available at the linac) the shape of the photon spectrum producing neutrons with energy less than 6 MeV should be well represented by the Schiff spectrum normally used in bremsstrahlung analysis[12] with a small correction for thick-target effects. Such effects are not completely negligible because the electrons are stopped in a carbon block which is only 12 in. from the deuterium sample. The deuterium sample used in this measurement was a cylindrical shell of deuterated polyethylene 4 mm thick, 4 cm o.d., and 4 cm high.

The efficiency function $g(E,77°)$ thus determined is shown in Fig. 6. The abscissa is neutron energy E in MeV and the ordinate scale is arbitrary. The points represent the deuterium data with the energy dependence of the photon spectrum taken to be the thin

[15] F. Partovi, Ph.D. thesis, Massachusetts Institute of Technology, 1962 (unpublished); Ann. Phys. (N. Y.) **27**, 79, 114 (1964).

[16] A. Donnachie, Nucl. Phys. **37**, 594 (1962); G. Kramer and D. Müller, Z. Physik **158**, 204 (1960).

[17] A summary of the experiments and results may be found in R. Wilson, *The Nucleon-Nucleon Interaction* (John Wiley & Sons, Inc., New York, 1963).

target shape; the solid curve is drawn by eye through the points; the dashed curve is the solid curve after correction for the thick-target effects and represents the form used in the reduction of the thorium data. The effective threshold for the detector in these experiments was about 0.6 MeV. The counter may be operated with a threshold as low as 0.25 MeV, but a higher threshold was used in this experiment in order to reduce background and since neutrons below 1 MeV did not necessarily come from fission and so were of no interest. The minimum in the efficiency at about 3.5 MeV and the structure below 2 MeV result from the transmission of the neutron spectrum through a considerable fraction of a mean free path of lead and bismuth.

The experimental results for $\rho_0 v^4$ for Th^{232} photofission, as computed from Eq. (4), are shown in Fig. 7. The data have been normalized to match the curve in the neighborhood of the peak. The curve will be described in the next section. The 7.75B data are not included in Fig. 7, since they are in essential agreement with the 7.75A data but somewhat inferior in both counting statistics and velocity resolution. The velocity resolution correction has not been applied to the data The resolution function of the apparatus is nearly rectangular with width equal to the separation between adjacent points in the presentation of Fig. 7. Including the effects of the grouping of the data, the resolution function with which to correct Fig. 7 is then an isosceles triangle with base equal to the separation of alternate points. This correction is small from the viewpoint of the purposes for which the data are used.

5. ANALYSIS OF THORIUM PHOTOFISSION DATA

In order to determine whether the data of Fig. 5 and Fig. 7 are consistent with the hypothesis of neutron emission from moving fragments, a prediction must be made in terms of a set of parameters obtained from either fission experiments on other elements or from the Th^{232} measurements themselves. The number of parameters is kept to a minimum by choosing a model in which neutron emission from fragments with a variety of masses, kinetic energies, and excitation energies (the various fission "modes") is replaced by emission from a typical heavy fragment and from a typical light fragment. These typical fragments have fixed velocities (V_H and V_L, respectively) representing the average velocity, weighted by the neutron-emission probability, of the actual heavy and light fragments. The respective contributions of the heavy and light fragments to the total number of neutrons are represented by ν_H and ν_L. The values for the V_H, V_L and ν_H, ν_L are taken from experience with other fissioning nuclei. It will be shown that the comparison with experiment for $\rho_0 v^4$ and ρ_2 is sensitive principally to the average of V_H and V_L. This quantity corresponds to the neutron-weighted average fragment kinetic energy per nucleon $\bar{E}_f$ which has been found to be 0 74±0.02 MeV for thermal-neutron fission of U^{233}, U^{235}, and Pu^{239} and for spontaneous fission of Cf^{252}.[5] The value of $\frac{1}{2}(V_H+V_L)$ chosen to represent Th^{232} photofission corresponds to $\bar{E}_f=0.74\pm0.03$ MeV. The ratios V_L/V_H and ν_L/ν_H are assumed to be 1.455 ±0.10 and 1.0±0.3, respectively.[5]

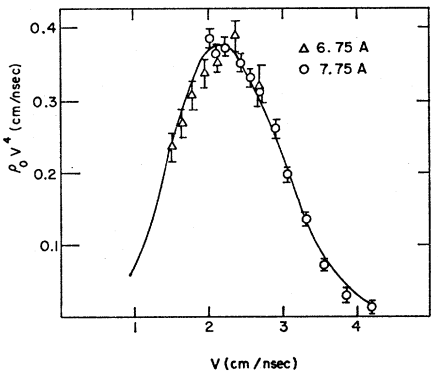

FIG. 7. $\rho_0 v^4$ versus neutron velocity v for Th^{232} photofission neutrons. This quantity is proportional to the total (integrated-over-angle) number of neutrons per unit interval of flight time. The curve represents a prediction for $\rho_0 v^4$ on the basis of isotropic evaporation from moving fragments. The points have been normalized to match the curve in the neighborhood of the peak.

It is assumed that the emission spectrum in the c.m. frame averaged over all fissions can be represented by an evaporation spectrum with some distribution of temperatures $P(T)$,

$$\varphi(\eta)=\eta\int_0^\infty P(T)\exp(-\eta/T)T^{-2}dT,$$

where $\varphi(\eta)d\eta$ is the fraction of neutrons with c.m. energy between η and $\eta+d\eta$. The average c.m. energy $\bar{\eta}$ is related to the average temperature $\bar{T}$: $\bar{\eta}=2\bar{T}$. We assume that $\bar{\eta}_L/\bar{\eta}_H=1.0\pm0.3$ and that the emission spectrum is the same for light and heavy fragments. It will be shown that predictions for ρ_0 and ρ_2 are not sensitive to these assumptions. With these conditions, the second central moment of the emission spectrum is related to the similar moment of the temperature distribution and to $\bar{T}$:

$$\sigma^2(\eta)/\bar{\eta}^2\equiv\langle(\eta-\bar{\eta})^2\rangle/\bar{\eta}^2=\tfrac{1}{2}+\tfrac{3}{2}\sigma^2(T)/\bar{T}^2.$$

Terrell[18] has described a simple method, based on statistical theory,[19] for predicting the general features of the temperature distribution $P(T)$. The initial excitation energy of the fragments is assumed to have a Gaussian distribution about an average value $(\bar{\nu}+1)E_0/2$, with an rms deviation $\sigma E_0/\sqrt{2}$. $\bar{\nu}$ is the average number of neutrons per fission, E_0 (about 6.7 MeV) is the average excitation change per emitted neutron, and σ may be estimated to be about 1.08 either from measured fragment kinetic energy distri-

[18] J. Terrell, Phys. Rev. **113**, 527 (1959).
[19] See, e.g., J. M. Blatt and V. F. Weisskopf, *Theoretical Nuclear Physics* (John Wiley & Sons, Inc., New York, 1952).

TABLE I. Sensitivity of angular moments of ρ to various parameters. A sensitivity index $x(\partial\rho_n/\partial x)$ is shown for each of the eight parameters which are important in determining ρ_n. The parameters x are defined in the text. The indices are given for the first five angular moments and for three values of the neutron velocity v. The evaluations were carried out for values of the x appropriate for the threshold photofission of Th^{232}. These values are shown in the table, and their sources indicated in the footnotes. The omission of entries at $v=1.4$ cm/nsec is discussed in the text. The values of the moments ρ_n are also given; ρ_0 is in units of $(\text{cm/nsec})^{-3}$.

	v (cm/nsec)	ρ_n	$x=\nu_L+\nu_H=2.4$	$x=\nu_L/\nu_H=1.0\pm0.3$[a]	$x=0.5\times(V_L+V_H)=1.180\pm0.025$ cm/nsec[a]	$x=V_L/V_H=1.455\pm0.1$[a]	$x=\bar{\eta}=1.14\pm0.06$ MeV[b]	$x=\bar{\eta}_L\ \bar{\eta}_H=1.0\pm0.3$[a]	$x=A_2-1=1.0\pm0.1$[c]	$x=\sigma^2(\eta)\ \bar{\eta}^2=0.77\pm0.06$[b]
$\partial\rho_0$	1.4	0.0505	1	−0.07	−0.9	−0.2	−0.5	+0.04	+0.20	+0.15
$x\rho_0^{-1}\frac{}{\partial x}$	2.2	0.0161	1	+0.09	+0.6	0.00	+0.25	−0.10	+0.05	−0.4
	3.0	0.00268	1	+0.15	+1.5	+0.2	+1.5	−0.03	−0.10	+0.03
$\partial\rho_1$	1.4	−0.13	0							
$x\frac{}{\partial x}$	2.2	0.45	0	+1.2	+0.09	+1.2	−0.6	−0.03	+0.04	+0.4
	3.0	0.89	0	+1.3	+1.7	+1.8	−0.9	+1.1	−0.04	−0.7
$\partial\rho_2$	1.4	1.15	0	+0.03	+0.06	−0.3	−0.8	+0.06	0.00	+0.9
$x\frac{}{\partial x}$	2.2	1.99	0	+0.15	+1.5	+0.06	−1.1	−0.04	−0.5	−0.10
	3.0	2.52	0	+0.14	+1.7	+0.24	−1.4	−0.02	−0.6	−1.0
$\partial\rho_3$	1.4	0.16	0							
$x\frac{}{\partial x}$	2.2	0.61	0	+0.6	+0.8	+1.4	−0.9	−0.5	−0.16	+0.8
	3.0	1.05	0	+0.8	+1.6	+2.1	−1.4	0.00	−0.4	−1.0
$\partial\rho_4$	1.4	0.08	0							
$x\frac{}{\partial x}$	2.2	0.70	0	+0.2	+1.5	+0.25	−1.2	−0.25	−1.7	+1.0
	3.0	1.18	0	+0.2	+2.2	+0.8	−1.8	−0.12	−1.6	−1.4

[a] Reference 5. [b] A result of this experiment. [c] See text.

butions or from neutron number distributions.[20] The distribution of residual excitation energy after the emission of the first neutron is estimated, then the distribution after the second emission, and then the distributions after the third and succeeding neutron emissions. These distributions in residual excitation energy E_r are summed and converted to $P(T)$ by use of the relation $T=(E_r/a)^{1/2}$, where a is the Weisskopf level-density parameter. The curve in Fig. 8 displays Terrell's prediction for $P(T)$ with $\bar{\nu}=2.46$ and $a=12$ MeV^{-1}. The $\bar{\nu}$ value should be a reasonable one for Th^{232} photofission and the density parameter is that required to obtain agreement with experimental values of $\bar{T}$ for various fissioning nuclides.[18] The three points which are also displayed in Fig. 8 are a result of the present experiment, and their justification is the subject of the next few paragraphs. They are to be interpreted as a histogram, and the upper edge of the highest temperature box has been placed in such a way that temperatures higher than this edge would be inconsistent with the data.

Two characteristics of $P(T)$ which are expected on the basis of the analysis described above are: (a) $P(T)$ is nearly proportional to T at low T, reflecting the fact that the distribution of residual excitation should be essentially flat over the first few MeV of excitation energy. (b) $P(T)$ should cut off sharply at about $T=2\bar{T}$, reflecting the relative improbability of either unusually high residual excitations or unusually low specific heats. Assuming that (a) is approximately correct, it is possible to obtain nearly independent answers to three questions concerning $P(T)$ from the data of Figs. 5 and 7. In the first place, a value of $\bar{T}$ (or, equivalently, $\bar{\eta}$) can be obtained from the measurement of $\rho_0 v^4$. Secondly, a value of $\sigma^2(T)$ [or, equivalently, $\sigma^2(\eta)/\bar{\eta}^2$] can be obtained from the velocity dependence of ρ_2 over the velocity range from about 1.7 to 2.7 cm/nsec provided that (b) is correct—that is, provided that there are no significant components of temperature higher than about $2\bar{T}$. Thirdly, the fact that there is no significant high-energy tail in the emission spectrum may be verified from the velocity dependence of ρ_2 for $v\gtrsim 2.7$ cm/nsec. Finally, with this knowledge of the c.m. emission spectrum, the comparison of predicted values with measured values of ρ_2 in the neighborhood of $v=2.2$ cm/nsec provides a check on the basic assumption of evaporation from moving fragments—that is, a measure of the fractional contribution of scission neutrons at this velocity.

The justification for the statements of the preceding paragraph and the assignment of experimental values for $\bar{\eta}$, for $\sigma^2(\bar{\eta})/\bar{\eta}^2$, and for the fraction of scission neutrons rests on several computer experiments. One of these is summarized in the curves of Figs. 5 and 7 and in Table I. The formulas which were used in the evapo-

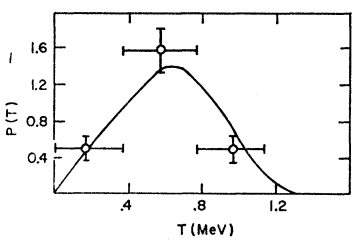

FIG. 8. Fragment temperature distribution for Th^{232}. The curve is taken from Fig. 6 of Ref. 18. The points are a result of the present experiment.

[20] J. Terrell, Phys. Rev. 108, 783 (1957).

ration predictions of $\rho(v,\theta)$ have been given in BTMS and are reproduced in the Appendix. For a given v, values of $\rho(v,\theta)$ were computed for 19 values of $\cos\theta$ equally spaced between -1 and 1. The appropriate angular integrations to determine ρ_0 and ρ_2 were then performed numerically (see the Appendix). The temperature distribution $P(T)$ was represented by three temperatures: $\bar{T}$, weighted by $(1-2\alpha)$; $\bar{T}+0.4$ MeV, weighted by α; and $\bar{T}-0.4$ MeV, weighted by α. Best values for the two parameters $\bar{T}$ and α were determined by comparison of the predictions with the data of Figs. 5 and 7. $\rho_0 v^4$ is not sensitive to α, and the best value of $\bar{T}$ (0.57 MeV) was determined from Fig. 7. Using this value of $\bar{T}$, a best value of α (0.18) was determined from the data of Fig. 5. The curves on Figs. 5 and 7 represent the predictions for ρ_2 and for $\rho_0 v^4$ using these best values for $\bar{T}$ and α. The shaded area in Fig. 5 represents $0.14<\alpha<0.22$ [which is equivalent to $0.71<\sigma^2(\eta)/\bar{\eta}^2<0.83$] for $\bar{T}=0.57$ MeV.

The sensitivity of the predictions to various parameters (call them x) was investigated by varying the x one at a time about the values which predict the curves of Figs. 5 and 7, recomputing the various moments, and estimating the quantities $x(\partial\rho_n/\partial x)$, which are useful sensitivity indicators. These indicators are presented in Table I for $v=1.4$, 2.2, and 3.0 cm/nsec and for the first five angular moments of ρ. Although the Th^{232} experiment is concerned only with ρ_0 and ρ_2, some experience with the other moments is useful in discussing the results of BTMS. The parameters x of Table I have been previously defined with the exception of A_2. A_2 characterizes the angular distribution of the neutrons in the c.m. frame (see the Appendix). A_2 is taken to be 0.0 ± 0.1 on the grounds that larger c.m. anisotropies than those corresponding to $|A_2|=0.1$ would be inconsistent both with the assumption of neutron evaporation[21] and with the data of BTMS (see later discussion).

An important feature of Table I is the insensitivity of ρ_0 and ρ_2 to the parameters which characterize the way in which fragment velocity, emission probability, and c.m. energy are distributed between light and heavy fragments. This insensitivity, along with the fact that there are two sharp peaks in the fragment mass distribution, constitutes the justification for the model which replaces the averaging of the emission process over all fission modes with emission by a typical light and heavy fragment possessing certain average properties. The odd angular moments and higher even moments are sensitive to these distribution parameters. This is particularly true for velocities near V_H and V_L. The sensitivities of ρ_1, ρ_3, and ρ_4 at 1.4 cm/nsec have been omitted in Table I, as the values would be misleading because of the proximity of $V_L=1.40$ cm/nsec.

In preparing Table I and determining best values for $\bar{\eta}$ and $\sigma^2(\eta)/\bar{\eta}^2$, we have assumed a temperature distribution $P(T)$ of the general form shown by the curve in Fig. 8—roughly symmetric and without any significant high-energy tail. Further computer experiments have shown that predictions as determined by $\bar{\eta}$ and $\sigma^2(\eta)/\bar{\eta}^2$ are not very sensitive to skewness of the peak in $P(T)$ near $\bar{T}$, but that predictions for ρ_2 at high velocities are very sensitive to the presence of temperatures equal to $\bar{\eta}$ and higher. This sensitivity will be illustrated later with reference to the Cf^{252} data of BTMS, which seem to require such high-temperature components. As far as the Th^{232} data are concerned, the agreement of the measured ρ_2 with the predictions at $v\gtrsim3$ cm/nsec appears to rule out any significant high-temperature tail in $P(T)$. Were such a tail present, it would be essentially indistinguishable from a scission neutron component, given only ρ_0 and ρ_2. If it is assumed that scission neutrons are isotropic in the laboratory, a fraction f of scission neutrons at a given velocity would reduce the values of all angular moments (except ρ_0) by $1-f$ from the value predicted in the absence of scission neutrons. In the neighborhood of $v=2.2$ cm/nsec, the predicted ρ_2 can be compared with that measured, and an estimate of the number of scission neutrons obtained which is nearly independent of uncertainties in the shape of the emission spectrum.

The analysis of the Th^{232} photofission data can be summarized as follows: The data can be understood on the basis of isotropic evaporation from moving fragments. The c.m. emission spectrum is characterized by $\bar{\eta}=1.14\pm0.06$ MeV and $\sigma^2(\eta)/\bar{\eta}^2=0.77\pm0.06$, and there are no significant components of temperature as high as or higher than $\bar{\eta}$. At about 2.2 cm/nsec (about 2.5 MeV) the fraction $f=0.07\pm0.09$ of the neutrons may be scission neutrons. Use has been made of Table I in assigning uncertainties. The uncertainty associated with the fraction of scission neutrons arises in roughly equal measure from the lack of precise knowledge of $\bar{\eta}$, of A_2, of a_2, of ϵ, and from counting statistics.

A quantitative statement with which our estimate of f may be compared is that of Skarsvåg and Bergheim.[3] A result of their neutron energy and angular distribution measurements for thermal neutron induced fission of U^{235} is that $15\%\pm1\%$ of the prompt neutrons are emitted isotropically in the laboratory, with an evaporation spectrum characterized by a temperature of 0.9 MeV. Given this spectrum, the contribution to ρ_0 of such a component for Th^{232} can be evaluated, yielding $f=0.16$ over a wide range of v centered about 2.2 cm/nsec. This result is just within the limits of error of our measurement of f. While considering possible differences between U^{235} thermal neutron fission and Th^{232} threshold photofission, it is perhaps important to recall that the photofission suppresses the symmetric fission modes. Fragment mass ratios near unity, normally rare, are particularly rare in photofission of even mass nuclides near threshold.[7] Symmetric fission in U^{235} seems to possess special characteristics with respect to neutron

[21] T. Ericson and V. Strutinski, Nucl. Phys. 8, 284 (1958), with errata, 9, 689 (1958/59).

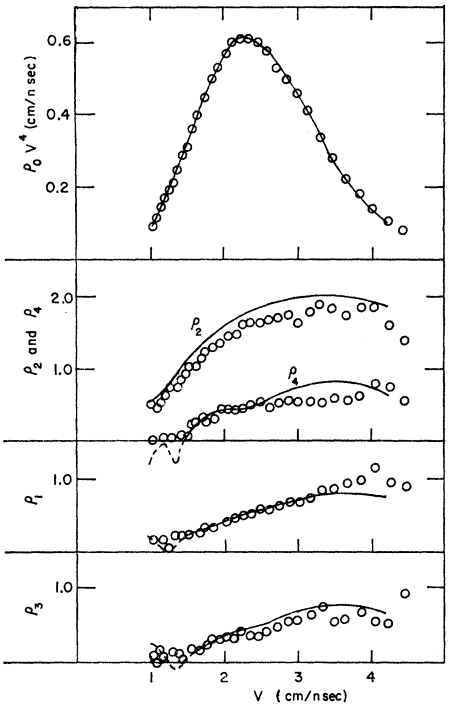

FIG. 9. Angular moments versus neutron velocity v for Cf^{252} spontaneous fission neutrons. The points are the data of BTMS (Ref. 1) integrated over angle as described in the Appendix. The curves are the result of a three-temperature isotropic evaporation prediction obtained by attempting to fit the data. The parameters used are given in the Appendix. Dashed curves are shown where meaningful comparisons between the points and the curves cannot be made (see text).

emission, producing large numbers of neutrons per fission[22] and small fragment kinetic energies.[23]

6. COMPARISON OF CALIFORNIUM AND THORIUM FISSION NEUTRON MEASUREMENTS

It is possible to compare $\rho_0 v^4$ and ρ_2 for Th^{232} photofission with the angular moments for Cf^{252} spontaneous fission. The appropriate angular integrals have been performed on the $\rho(v,\theta)$ data reported in BTMS in order to determine the moments. Figure 9 displays "experimental points" for $\rho_0 v^4$, ρ_1, ρ_2, ρ_3, and ρ_4 obtained in this way. The method of numerical integration is described in the Appendix. We have attempted to fi' the Cf^{252} data expressed in angular moment form with a three-temperature evaporation prediction, and the curves in Fig. 9 represent the best fit obtained. The parameters used are given in the Appendix. The curves are dashed for the region of velocity near V_H and V_L where the comparison of curves and points is not meaningful. In addition to the difficulties of the model in this region discussed earlier with reference to the omission of certain entries from Table I, the numerical angular integration and data extrapolation procedures are inadequate because of the rapid angular and velocity variation of ρ near 0° and 180°. The scale for the prediction of $\rho_0 v^4$ in Fig. 9 has been determined by choosing $\nu = 3.77$, the recent result of Hopkins and Diven.[24] Although it is possible to obtain a good fit to $\rho_0 v^4$, it does not seem to be possible to fit ρ_2 and ρ_4. The points for these moments generally lie a few percent low as did the measurements for ρ_2 in the case of Th^{232} photofission. This is the situation that one would expect if a few percent of scission neutrons were present in addition to the majority evaporated from moving fragments.

The moments ρ_1, ρ_3, and ρ_4, which were not available for Th^{232} photofission, have some interesting properties. The odd moments are quite sensitive to ν_L/ν_H. The value 1.26 for this ratio used in the predictions of Fig. 9 is a choice which is consistent with the data. It would require further investigation, however, to determine the extent to which this model parameter actually represents the ratio of the average numbers of neutrons emitted by the light and heavy fragments. Also, at high velocities ρ_1 is very sensitive to the parameter $\bar{\eta}_L/\bar{\eta}_H$, whereas the other moments (including ρ_3) are not. The prediction has assumed the same c.m. spectrum for light and heavy fragments. The apparent inconsistency at high velocities of ρ_1 with the rest of the data is then evidence that the spectrum from the light fragment is weighted more toward high energies than the heavy fragment spectrum. This is to be expected (see discussion of Fig. 11 below). Finally, an important feature of ρ_4 is its great sensitivity to A_2, the parameter characterizing the angular distribution of neutron emission in the c.m. frame (see Table I). Were A_2 equal to 0.1 rather than 0.0, the prediction for ρ_4 would be increased by about 0.15 for all velocities greater than about 1.4 cm/nsec. The same change does not affect significantly the prediction for ρ_2 below about 2 cm/nsec and the effect on ρ_2 is relatively small even at 4 cm/nsec. The approximate agreement of the points with the prediction for ρ_4 in Fig. 9 can be accepted as

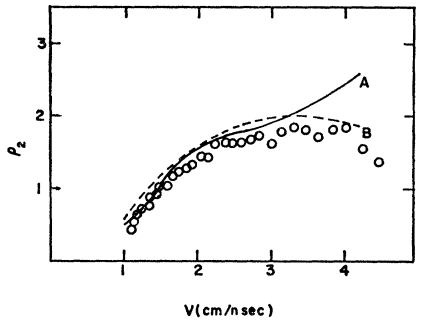

FIG. 10. ρ_2 versus neutron velocity v for Cf^{252}. The points and curve B are the experimental data and isotropic evaporation prediction reproduced from Fig. 9. Curve A represents the prediction obtained from the parameters of line 1 in Table VI of BTMS (1962).

[22] V. F. Apalin, Yu. N. Gritsyuk, I. E. Kutikov, V. I. Lebedov, and L. A. Mikaélyan, Zh. Eksperim. i Teor. Fiz. 43, 329 (1962) [English transl.: Soviet Phys.—JETP 16, 235 (1963)].

[23] J. C. D. Milton and J. S. Fraser, Can. J. Phys. 40, 1626 (1962).

[24] J. C. Hopkins and B. C. Diven, Nucl. Phys. 48, 433 (1963).

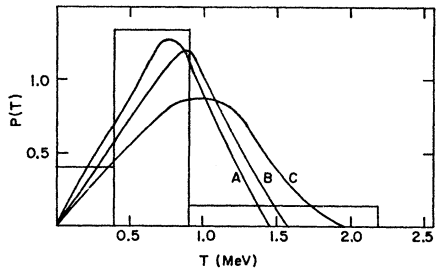

FIG. 11. Fragment temperature distributions for Cf^{252}. The histogram represents the three temperatures and weighting fractions used in Fig. 9. Curve A is taken from Fig. 6 of Ref. 18. Curves B (for the heavy fragment) and C (for the light fragment) were calculated by a similar method, using Cameron's prescription for level densities (Ref. 25) and the result of Ref. 1 for the average initial excitation energy as a function of mass number.

evidence that the neutron emission is very nearly isotropic in the c.m. frame.

The predictions shown in Fig. 9 are very similar, below about 3.5 cm/nsec, to the curves obtained from the parameters given as the best fits to the Cf^{252} data [e.g., line 1 of Table VI in BTMS (1962)], even though the two sets of temperatures and weighting factors are quite different. However, at high velocities the BTMS parameters fail to represent the data well. This is most clearly seen by examining ρ_2. In Fig. 10, curve A is the prediction based on the best fit of BTMS mentioned above; the parameters are listed in the Appendix. The c.m. spectrum for this curve has $\bar{\eta}=1.44$ MeV and $\sigma^2(\eta)/\bar{\eta}^2=0.79$. The experimental data and our best fit (curve B) are reproduced from Fig. 9 for comparison. The c.m. spectrum for curve B has $\bar{\eta}=1.48$ MeV and $\sigma^2(\eta)/\bar{\eta}^2=0.95$, and also differs markedly from curve A in the higher moments of the spectrum. B has an evaporation component with a temperature of 1.56 MeV, whereas A has no component of temperature greater than 0.99 MeV. The flat velocity dependence of ρ_2 at high velocities as seen in curve B is characteristic of c.m. spectra with high-energy tails.

The most apparent difference between the Th^{232} and Cf^{252} fission-neutron spectra is that the Cf^{252} data seems to require a significant contribution from temperatures of the order of $\bar{\eta}$ while the Th^{232} data do not. The presence of this high-energy tail in the spectrum representing the average over all modes implies neither that there is a tail in the spectrum from any individual fission fragment nor that the shape of the c.m. spectrum depends on the mass number A. The term "shape" is used as defined in BTMS. It refers to the normalized to-unity distribution in the dimensionless variable $\eta/\bar{\eta}$. The tail in the averaged-over-modes spectrum can result from the strong A-dependence of the average c.m. energy of the neutrons emitted by a given fragment. This effect is illustrated by Fig. 11. The histogram in Fig. 11 represents the three-temperature best fit of Fig. 9. Curve A represents Terrell's prediction for $P(T)$ with $\bar{\nu}=3.86$ and $a=12$ MeV^{-1}.[18] We have calculated curves B and C using similar methods, but making use of Cameron's prescription for level densities[25] and that of BTMS for average initial excitation energy as a function of mass number [see Fig. 22 of BTMS (1963)]. Curve B is the predicted temperature distribution for heavy fragments and curve C that for light fragments. The average temperature for B and C is considerably higher than that for A. This is the result, for the most part, of the lower average values of a prescribed by Cameron. The interesting feature of the curves is the high-energy tail of the light-fragment distribution C. This tail comes from the high side of the mass distribution peak—that is, the region $110<A<125$—characterized by large initial fragment excitation energies and high neutron multiplicities. The magnitude of the high-energy tail in the average emission spectrum would be quite sensitive to effective level densities in this mass region.

7. SUMMARY

The results of the Th^{232} photofission experiment support the point of view that threshold photofission is no different from other threshold fission processes with respect to prompt neutron emission. The measured neutron distribution in energy and angle is consistent with the hypothesis that most of the neutrons result from isotropic emission from fully accelerated fragments. The c.m. neutron spectrum is well represented by an evaporation-type spectrum with a distribution of temperatures. The average energy and width of the spectrum are in accord with what might be expected on the basis of other fission experiments on neighboring nuclei.[5]

The observed difference between the Cf^{252} c.m. neutron spectrum integrated over fragment mass and that for Th^{232}—the pronounced high-energy tail in the former and the absence of such a tail in the latter—can probably be understood in terms of the mass yield curve for the two nuclides. It has been noted that the fragment-mass region $110<A<125$ is associated with unusually high excitation energies and neutron multiplicities. This mass region is well sampled by Cf^{252} spontaneous fission and is essentially not at all represented in Th^{232} threshold photofission.

The present analysis of the data for Th^{232} and of the data of BTMS for Cf^{252} is consistent with a contribution of a few percent of neutrons isotropic in the laboratory, as was apparently also observed in thermal neutron induced fission of U^{235}.[2,3] More precise information concerning these minority "scission neutrons" will be difficult to obtain. It will require a good understanding of the majority "fission neutrons"—those neutrons emitted from moving fragments. Knowledge of the high-energy part of the fission neutron emission spectrum in the fragment center-of-mass frame is particularly relevant to answering questions concerning scission neutrons,

[25] A. G. W. Cameron, Can. J. Phys. 36, 1040 (1958).

and determining this spectrum with the necessary accuracy poses a difficult experimental problem.

APPENDIX

Predictions of $\rho(v,\theta)$ have been made on the basis of the model described in Sec. 5. The appropriate formulas have been presented in BTMS(1962) and are reproduced below.

$$\rho(v,\theta)=\rho_L+\rho_H,$$

where L and H refer to light and heavy fragments, respectively.

$$\rho_I=(2a^2/4\pi)u_I\nu_I B_I\sum_i(\alpha_{iI}/T_{iI}^2)\exp(-au_I^2/T_{iI}),$$

where I refers to L or H. v is the velocity (lab) of the neutrons (cm/nsec), θ is the laboratory angle between the neutron and the light fragment, $a=0.5228=$ (neutron energy in MeV)/v^2, u is the neutron velocity (cm/nsec) in the fragment center-of-mass frame, ν_I is the number of neutrons per fission from the appropriate fragments. T_i are temperatures pertaining to the center-of-mass energy distribution and α_i the corresponding weighting fractions: $\sum_i\alpha_{iI}=1$. $B=1-A_2P_2(\cos\psi)$, with A_2 a parameter characterizing the center-of-mass angular distribution of neutrons, and ψ the center-of-mass angle between neutrons and fragments.

The following relations were used to obtain u and $\cos\psi$:

$$u_L^2=v^2+V_L^2-2vV_L\cos\theta,$$
$$u_H^2=v^2+V_H^2+2vV_H\cos\theta,$$
$$\cos\psi_L=(v\cos\theta-V_L)/u_L,$$
$$\cos\psi_H=(-v\cos\theta-V_H)/u_H.$$

V_H and V_L are the neutron-weighted average velocities of the heavy and light fragments, respectively.

TABLE II. Parameters used in calculating curves displayed in Figs. 5, 7, 9, and 10.

	V_L (cm/nsec)	V_H (cm/nsec)	T_1 (MeV)	T_2 (MeV)	T_3 (MeV)	α_1	α_2	α_3	ν_L	ν_H
Th^{232} Figs. 5 and 7	1.40	0.96	0.97	0.57	0.17	0.18	0.64	0.18	1.2	1.2
Cf^{252} Fig. 9 and Fig. 10, curve B	1.34	1.02	1.560	0.664	0.193	0.170	0.670	0.160	2.10	1.67
Cf^{252} Fig. 10, curve A	1.34	1.02	0.994	0.373	0.073	0.572	0.406	0.022	1.97	1.70

The angular moments ρ_n of ρ are defined by

$$\rho(v,\theta)=\rho_0(v)[1+\sum_{n=1}^{\infty}\rho_n(v)P_n(\cos\theta)],$$

or

$$\rho_0(v)=\frac{1}{2}\int_{-1}^{1}\rho(v,\theta)d(\cos\theta),$$

$$\rho_n(v)=[(2n+1)/2\rho_0]\int_{-1}^{1}\rho(v,\theta)P_n(\cos\theta)d(\cos\theta),\quad n\neq 0.$$

The angular integrations to determine the ρ_n were done numerically. For the desired value of v, $\rho(v,\theta)$ was calculated for 19 values of $\cos\theta$ equally spaced between -1 and $+1$. The integrations were then performed using Weddle's rule.[26]

[26] H. Margenau and G. M. Murphy, *The Mathematics of Physics and Chemistry* (D. Van Nostrand Co., Inc., New York, 1943), p. 461.

"Experimental values" of the ρ_n for Cf^{252} were obtained by performing the same numerical integrations, but with the 19 values of ρ for a given v obtained by interpolation (or, occasionally, extrapolation) of the measured values of ρ given in Tables IV and V of BTMS(1962). The interpolations and extrapolations were carried out linearly in $\cos\theta$.

Table II shows the model parameters which were used in the calculation of the curves which have been presented in Figs. 5, 7, 9, and 10. For all the curves $A_2=0$, and three-temperature evaporation spectra were used, with identical spectra for light and heavy fragments. Thus, nine parameters (V_L, V_H, T_1, T_2, T_3, α_1, α_2, ν_L, and ν_H) define a particular prediction. A tenth, $\alpha_3=1-(\alpha_1+\alpha_2)$, is also tabulated.